RSC Advances

PAPER

View Article Online
View Journal | View Issue

Cite this: *RSC Adv.*, 2022, **12**, 8945

Theoretical investigation of $FAPbSnGeX_3$ efficiency

H. Moatassim,*[a] H. Zaari,[a] A. El Kenz,[a] A. Benyoussef,[b] M. Loulidi[a] and O. Mounkachi*[ac]

The use of hybrid lead halide perovskites as light absorbers in photovoltaic cells have gained large interest due to their optoelectronic properties and high efficiency. However, most hybrid perovskites contain toxic lead which has a negative impact on the environment. In this work, we systematically study the structural, electronic, and optical properties of lower lead halide perovskites $FAPb_{0.5}Sn_{0.25}Ge_{0.25}X_3$ (X = I, Br, Cl), as well as discussing their photovoltaic performance (open circuit voltage (V_{oc}), the short circuit current density (J_{sc}), and the power conversion efficiency (η)) using density functional theory (DFT), and we compare these with $FAPbX_3$ (X = I, Br, Cl) frameworks. The compounds show a suitable band gap for photovoltaic applications, in which iodine has a lower gap value compared to chlorine. It is noteworthy that we found that lead doping by both germanium and tin in the $FAPb_{0.5}Sn_{0.25}Ge_{0.25}X_3$ (X = I, Br, Cl) materials significantly improves the adsorption coefficient and the stability of these systems compared to the $FAPbX_3$ (X = I, Br, Cl) systems. The calculated *Jsc* shows a monotonical decrease from $FAPb_{0.5}Sn_{0.25}Ge_{0.25}I_3$ to $FAPbCl_3$, which represents the lowest *Jsc*. Results reveal that $FAPb_{0.5}Sn_{0.25}Ge_{0.25}Cl_3$ demonstrates promising potential for photovoltaic application as it shows the highest efficiency. This study can help reduce the toxicity of hybrid lead halide perovskites and also raises their experimental power conversion efficiency.

Received 17th January 2022
Accepted 5th March 2022

DOI: 10.1039/d2ra00345g

rsc.li/rsc-advances

1. Introduction

The energy requirement has grown during recent years with the increase of human population and elevated consumption.[1–3] Solar energy represents an alternative to limit the use of fossil fuels and is a fast growing energy technology abundantly available.[4,5] Recently, organic–inorganic hybrid lead halide perovskite materials with the general formula ABX_3 (A = MA, FA, EA; B= Pb, Sn, Ge, Be; X= I, Br, Cl) have demonstrated great potential in different applications, especially photovoltaics.[6–9] The high efficiency represented by these materials has reached a value of 25.6% in a few years.[10] This rise has come from the unique properties of hybrid lead halide perovskites, such as a high absorption coefficient in the visible range, tunable bandgap, low effective mass, high carrier mobility.[11–14] Currently, a lot of parameters reduce the hybrid perovskite efficiency performance in solar cells. The defects are in the hybrid perovskite structure, toxicity, and their degradation in the presence of ultraviolet light, humidity and oxygen.[15–18]

Iodine migration in hybrid perovskites creates structure defects which can be the cause of the current voltage hysteresis.[19] Also, hybrid perovskite degradation under ultraviolet light has a direct relation to iodine oxidation; it has been demonstrated that iodine doping by bromine is a solution to limit this degradation.[20,21] The choice of the organic cation in the hybrid perovskite also plays a major role in the material performance.[22] Oranskaia *et al.* have demonstrated that ions have a lot more space to migrate in the $MAPbBr_3$ structure than the $FAPbBr_3$,[23] as the H-bonding in MA and FA has an effect on the stabilization of the halogen vacancies. Other work has demonstrated that hydrogen vacancies can be present in $MAPbI_3$ with high densities, in contrast with $FAPbI_3$ where they are difficult to form and make the $FAPbI_3$ more stable and higher performing in photovoltaic applications.[24] On the other hand, the high efficiency achieved by hybrid perovskites shown by lead halide perovskites is counteracted by their toxicity,[25,26] which blocks the commercialization of these compounds. The substitution of lead by tin in both $FAPbI_3$ and $MAPbI_3$ has demonstrated an efficiency of 5.51% and 3.13%, respectively,[27] while the substitution of lead by Ge in $MAPbI_3$ shows an efficiency of 0.2% and $FAGeI_3$ does not show any photocurrent.[28] A theoretical study has demonstrated that the partial substitution of lead by both tin and germanium shows a high performance in photovoltaic applications.[29] So far no substitution of lead has demonstrated better performance than $MAPbI_3$. In this work, we studied the lower levels of free lead halide perovskite $FAPb_{0.25}Sn_{0.25}Ge_{0.25}X_3$ (X= I, Cl and Br) using density functional theory, where the lead was doped with both Sn and Ge, and compared with the photovoltaic results of the $FAPbX_3$ (X = I, Br,

---

[a] Laboratory of Condensed Matter and Interdisciplinary Sciences (LaMCScI), Faculty of Science, Mohammed V University in Rabat, Morocco. E-mail: hajarmoatassim1@gmail.com; omar.mounkachi@um5r.ac.ma

[b] Hassan II Academy of Science and Technology, Rabat, Morocco

[c] MSDA, Mohammed VI Polytechnic University, Lot 660, Hay Moulay Rachid Ben Guerir, 43150, Morocco

Cl) compounds. The structural, electronic and optical properties of these compounds were investigated, and we discuss their power conversion efficiency. For this purpose, the photovoltaic parameters, open circuit voltage and the short circuit current density were investigated.

2. Computational methods

In this work, density functional theory implemented in the quantum espresso code was used to study the structural and electronic properties of $FAPbX_3$ (X = I, Br, Cl), and $FAPb_{0.5}Sn_{0.25}Ge_{0.25}X_3$ (X= I, Cl and Br) compounds.[30] The structure optimization of tetragonal $FAPb_{0.5}Sn_{0.25}Ge_{0.25}X_3$ was carried out using Normcons type pseudopotentials in which the Martins–Troullier method was employed, as well as a functional type Perdew–Burke–Ernzerhof (PBE) exchange correlation nonlinear non-relativistic core correction. A 65 Ry plane wave cut off with a $6 \times 6 \times 5$ *k*-mesh was used to optimize the unit cell. The van der Waals-DFT (vdw-df-ob86) approximation was used for the exchange–correlation functional[31] as it gives accurate results that match the experimental data.[32] The optical properties of $FAPbX_3$ and $FAPb_{0.5}Sn_{0.25}Ge_{0.25}X_3$ were calculated using the Yambo code.[33]

To estimate the photovoltaic performance of each compound, the conversion efficiency was calculated using the following equation:[34]

$$\eta = \frac{V_{oc} \times J_{sc} \times FF}{P_{in}} \times 100 \quad (1)$$

where the fill factor FF has been calculated using the following equation:[35]

$$FF = \frac{\upsilon_{oc} - \ln(\upsilon_{oc} + 0.72)}{\upsilon_{oc} + 1} \quad (2)$$

υ_{oc} is defined as a "normalized V_{oc}":

$$\upsilon_{oc} = \frac{q}{kT} V_{oc} \quad (3)$$

P_{in} represents the light power density of incident light on the solar cell in this work under the standard test conditions ($T = 25°$, AM1.5G) equal to 1000 W m^{-2}, V_{oc} represents the open circuit voltage that can be expressed for perovskites solar cells as follows:

$$eV_{oc} = E_g - E_{loss}; E_{loss} = 0.7 \text{ or } 0.5 \text{ eV} \quad (4)$$

where E_{loss} represents a variable parameter potential loss.[36]

The short circuit current density J_{sc} was calculated using the following equation:[37]

$$J_{sc} = \int_{E1}^{E2} \Phi(E) Q_E(E) dE \quad (5)$$

where $\Phi(E)$ is the spectral irradiance (AM 1.5G) and $Q_E(E)$ is the quantum efficiency calculated by the equation:

$$Q_E = (1 - R(E))(1 - e^{-\alpha(E)t}) \quad (6)$$

Table 1 Lattice parameters and formation energy of $MAPbI_3$, $FAPb_{0.5}Sn_{0.25}Ge_{0.25}X_3$, and $FAPbX_3$ structures

Compounds	*a* (Å)	*b* (Å)	*c* (Å)	$E_{formation}$ (eV Å^{-1})
$MAPbI_3$	8.75	8.77	12.89	−4.26
$FAPb_{0.5}Sn_{0.25}Ge_{0.25}I_3$	8.89	8.84	12.34	−4.66
$FAPb_{0.5}Sn_{0.25}Ge_{0.25}Br_3$	8.42	8.36	11.58	−4.8
$FAPb_{0.5}Sn_{0.25}Ge_{0.25}Cl_3$	8.10	8.04	11.14	−4.93
$FAPbI_3$	8.99	8.99	12.72	−4.66
$FAPbBr_3$	8.47	8.47	11.98	−4.76
$FAPbCl_3$	8.17	8.17	11.26	−4.93

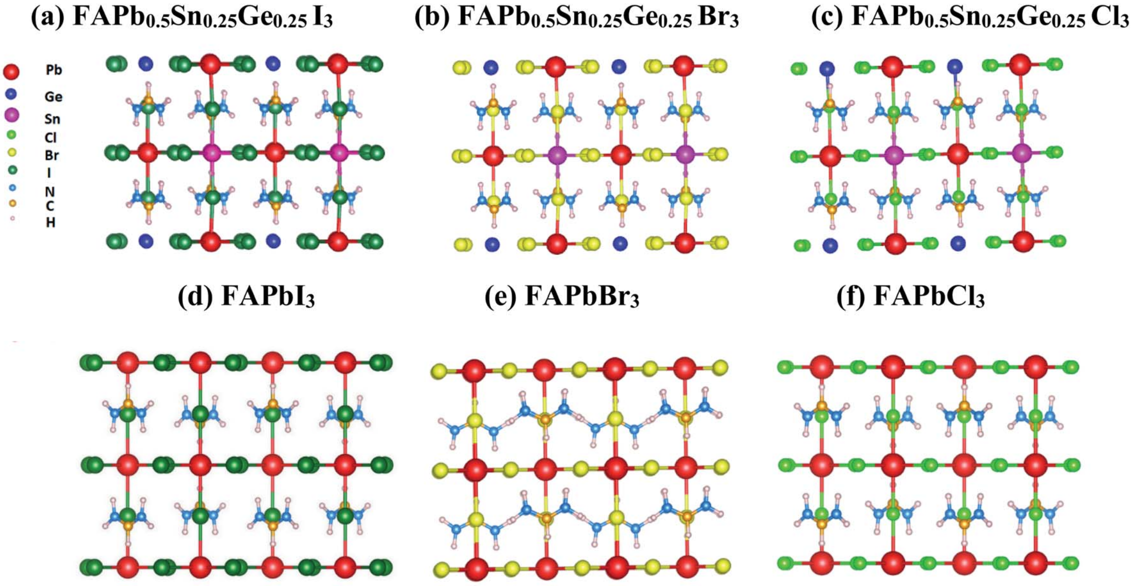

Fig. 1 Optimized tetragonal structures of $FAPb_{0.5}Sn_{0.25}Ge_{0.25}X_3$ and $FAPbX_3$.

R is the reflectivity, $\alpha(E)$ is the absorption coefficient and t is the thickness of the sample.

3. Results and discussion

3.1 Crystalline structure

The $FAPb_{0.5}Sn_{0.25}Ge_{0.25}X_3$ structures were created by the substitution of 50% of the lead (Pb) in $FAPbI_3$ with 25% of tin (Sn) and 25% of germanium (Ge). The halogens used were iodine, bromine, and chlorine. The optimized tetragonal structures and lattice parameters calculated for the $MAPbI_3$, $FAPbX_3$ and $FAPb_{0.5}Sn_{0.25}Ge_{0.25}X_3$ compounds are represented in Fig. 1 and Table 1, respectively. Table 1 shows clearly that the substitution of MA with FA changes the lattice from $a = 8.75$ Å to $a = 8.99$ Å due to the geometry of FA. The lattice parameters have been reduced with the substitution of half of the lead by tin and germanium, and further reduced with the use of bromine or chlorine. The calculated lattice parameters of $MAPbI_3$, and $FAPbX_3$ are in good agreement with previous experimental and theoretical reports.[38–41]

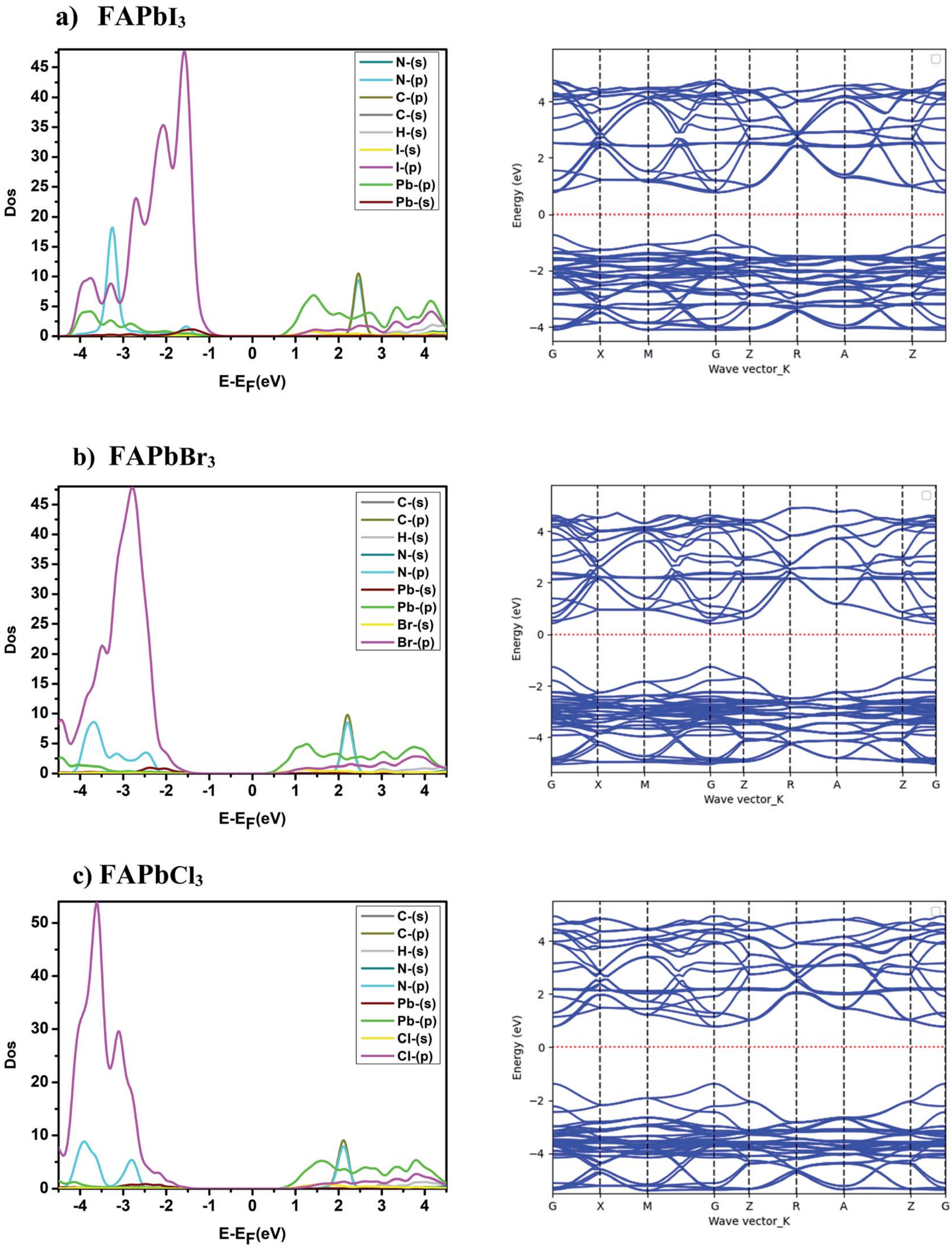

Fig. 2 Band structure and partial state density of $FAPbX_3$.

3.2 Electronic structure

The electronic structure study of the compounds consists of analyzing the partial density of states, the band structure and the effective mass. The band structures and the partial state density of the $FAPbX_3$, and $FAPb_{0.5}Sn_{0.25}Ge_{0.25}X_3$ compounds are presented in Fig. 2 and 3. The band structures show semiconductor character with a direct bandgap in the gamma points of the Brillouin zone. The difference between the band structures appears in the gap between the valence band maximum and the conduction band minimum. The calculated energy gap of the $FAPbX_3$ frameworks are 1.5 eV, 1.67 eV, and 2.14 eV for $FAPbI_3$, $FAPbBr_3$, and $FAPbCl_3$, respectively. The valence of $FAPbX_3$ is formed by the p-orbital of the halogen (I, Br, Cl) while the p-orbital of Pb formed the conduction band. The calculated effective mass of each structure is listed in Table 2. $FAPbCl_3$ presents a larger gap compared to the other compounds, a larger effective mass of electrons (Table 2) and therefore a low mobility. The latter improves its performance for photovoltaic

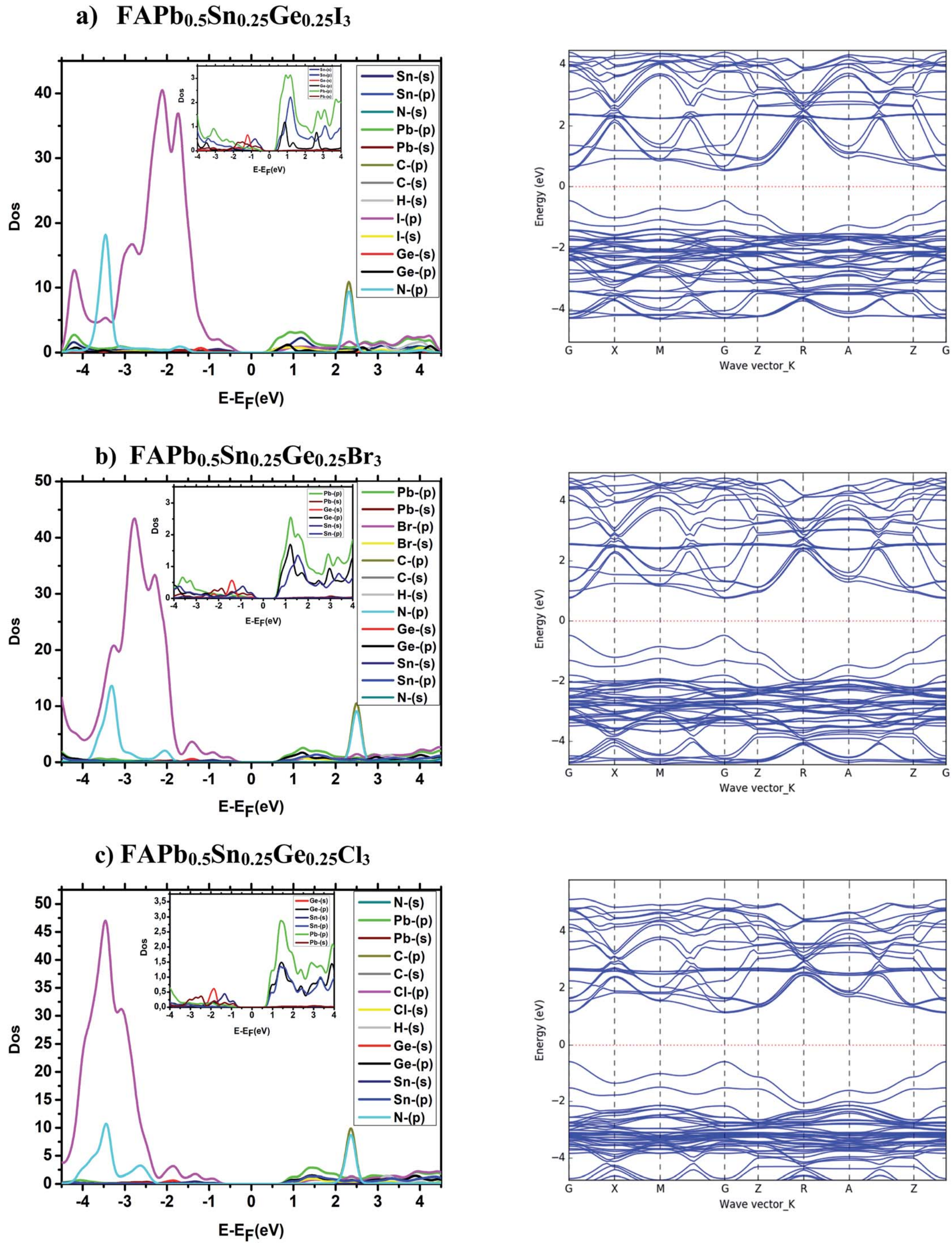
a) $FAPb_{0.5}Sn_{0.25}Ge_{0.25}I_3$

b) $FAPb_{0.5}Sn_{0.25}Ge_{0.25}Br_3$

c) $FAPb_{0.5}Sn_{0.25}Ge_{0.25}Cl_3$

Fig. 3 Band structure and partial state density of $FAPb_{0.5}Sn_{0.25}Ge_{0.25}X_3$.

Table 2 Effective mass of $MAPbI_3$, $FAPb_{0.5}Sn_{0.25}Ge_{0.25}X_3$, and $FAPbX_3$ structures

Compounds	E_g (eV)	m_e	m_h
$MAPbI_3$	1.6	0.19	0.34
$FAPb_{0.5}Sn_{0.25}Ge_{0.25}I_3$	0.98	0.29	0.07
$FAPb_{0.5}Sn_{0.25}Ge_{0.25}Br_3$	1.22	0.24	0.08
$FAPb_{0.5}Sn_{0.25}Ge_{0.25}Cl_3$	1.7	1.13	0.36
$FAPbI_3$	1.5	0.44	0.19
$FAPbBr_3$	1.67	0.35	0.11
$FAPbCl_3$	2.14	0.72	0.19

applications through the doping of Pb by Sn and Ge, which modified the electronic structures and electronic properties, and slightly altered the energy gap. The above will be discussed in the following.

The electronic properties of the lower free lead halide perovskite $FAPb_{0.5}Sn_{0.25}Ge_{0.25}X_3$ where the lead was doped with both Sn and Ge, are depicted in Fig. 3. The band structures represent a band gap of 0.98 eV, 1.22 eV and 1.7 eV for $FAPb_{0.5}Sn_{0.25}Ge_{0.25}I_3$, $FAPb_{0.5}Sn_{0.25}Ge_{0.25}Br_3$ and $FAPb_{0.5}Sn_{0.25}Ge_{0.25}Cl_3$, respectively. The valence band maximum (VBM) and the conduction band minimum (CBM) for both compounds $FAPb_{0.5}Sn_{0.25}Ge_{0.25}I_3$ and $FAPb_{0.5}Sn_{0.25}Ge_{0.25}Br_3$ shows a curvature indicating the low effective mass of carriers (electron–hole). In contrast the bands of the $FAPb_{0.5}Sn_{0.25}Ge_{0.25}Cl_3$ structure are almost flattened, thus the effective mass is greater when compared to the two other compounds as represented in Table 2. The $FAPb_{0.5}Sn_{0.25}Ge_{0.25}I_3$, $FAPb_{0.5}Sn_{0.25}Ge_{0.25}Br_3$ structures have an effective hole mass, lower than $MAPbI_3$. The effective mass is inversely proportional to the mobility of the carriers, therefore the mobility of the carriers of $FAPb_{0.5}Sn_{0.25}Ge_{0.25}I_3$ and $FAPb_{0.5}Sn_{0.25}Ge_{0.25}Br_3$ are large which will allow the electrons to easily cross the band gap. The CBM is mainly contributed by the p orbital of Pb in the $FAPb_{0.5}Sn_{0.25}Ge_{0.25}I_3$ structure, while it is dominated by the p orbital of the three elements Pb, Ge and Sn for the $FAPb_{0.5}Sn_{0.25}Ge_{0.25}Br_3$ and $FAPb_{0.5}Sn_{0.25}Ge_{0.25}Cl_3$. The VBM of the $FAPb_{0.5}Sn_{0.25}Ge_{0.25}X_3$ structures do not show any obvious difference, it is mainly derived from the p orbital of I, whereas the deep valence band is mainly contributed by the p orbital of N and the s orbital of Pb, Ge and Sn. The organic cation is positioned far from the VBM and the CBM. We notice that the co-doping of both Sn, and Ge elements shift the p states of halogen (I, Br, Cl) towards the lowest levels, which has reduced the gap energies, this doping also adds additional energy levels which will allow more optical transitions.

3.3 Optical properties

The absorption coefficient determines how far into a material light of a particular wavelength can penetrate before it is absorbed. The absorption coefficient and the reflectivity of the three compounds were calculated from the dielectric constant $\varepsilon = \varepsilon_1 + i\varepsilon_2$, where ε_1 and ε_2 represent the real and imaginary part of the dielectric function, respectively.

As Shown in Fig. 4, $FAPbI_3$ has a larger absorption coefficient in the visible spectra than $FAPbCl_3$ and $FAPbBr_3$, the co-doping with Sn and Ge improves the optical properties. As can be seen from the same figure, the three $FAPb_{0.5}Sn_{0.25}Ge_{0.25}X_3$ compounds have a high absorption coefficient in the visible range where the $FAPb_{0.5}Sn_{0.25}Ge_{0.25}I_3$ structure shows the highest absorption; while the $FAPb_{0.5}Sn_{0.25}Ge_{0.25}Br_3$ and $FAPb_{0.5}Sn_{0.25}Ge_{0.25}Cl_3$ structures revealed the best absorption coefficient in the ultraviolet region. In physics and electrical

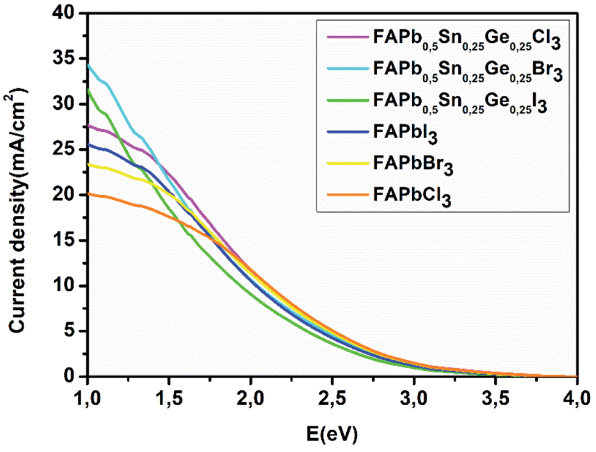

Fig. 5 Short-circuit current density of $FAPbX_3$, and $FAPb_{0.5}Sn_{0.25}Ge_{0.25}X_3$.

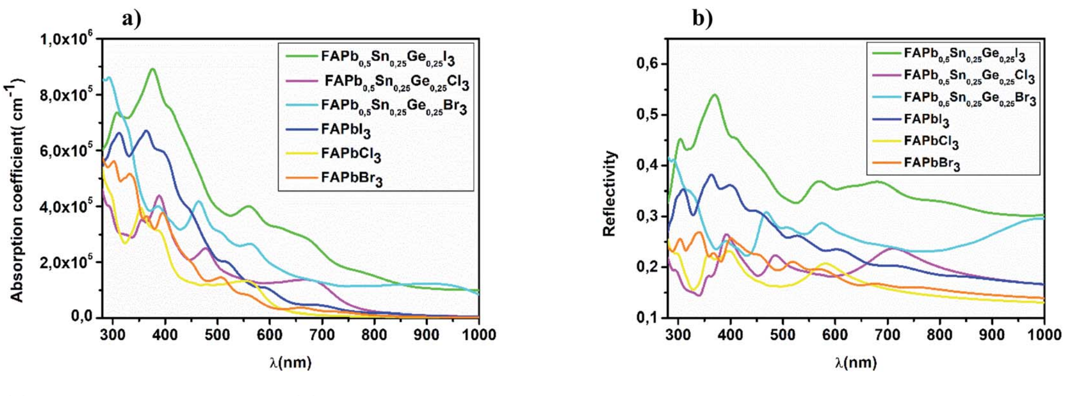

Fig. 4 Spectral (a) absorption coefficient and (b) reflectivity of $FAPb_{0.5}Sn_{0.25}Ge_{0.25}X_3$.

Table 3 The calculated bandgap E_g, short-circuit current density J_{sc}, open circuit voltage V_{oc} and power conversion efficiency η of $FAPb_{0.5}Sn_{0.25}Ge_{0.25}X_3$ structures

		V_{oc}			η%	
Compounds	E_g	E_{loss} (0.7 eV)	E_{loss} (0.5 eV)	J_{sc}	E_{loss} (0.7 eV)	E_{loss} (0.5 eV)
$FAPb_{0.5}Sn_{0.25}Ge_{0.25}I_3$	0.98	0.28	0.48	31.5	6.17	12
$FAPb_{0.5}Sn_{0.25}Ge_{0.25}Br_3$	1.22	0.52	0.72	29	12	17.5
$FAPb_{0.5}Sn_{0.25}Ge_{0.25}Cl_3$	1.7	1	1.2	18	15.8	19.3
$FAPbI_3$	1.5	0.8	1	20.3	14	17.8
$FAPbBr_3$	1.67	0.97	1.17	17.3	14.6	18
$FAPbCl_3$	2.14	1.44	1.64	9.6	12.5	14.3

engineering, the reflection coefficient describes how much of a wave is reflected by an impedance discontinuity in the medium transmission. According to Fig. 4b, all the investigated perovskite materials show a medium reflectivity in the IR-visible-UV region of the spectra. This reflectivity suggests that the materials have high absorptivity and/or transmissivity. Absorption coefficient and the reflectivity are the main parameters for the calculation of the short circuit current density.

3.4 Power conversion efficiency

The power conversion efficiency of solar cells is related to the material's electronic and optical properties. In order to calculate the efficiency of these compounds we first start by determining the photovoltaic parameters: short-circuit current density and open circuit voltage. The calculated power conversion efficiency (η) of $MAPbI_3$ with an open circuit voltage (V_{oc}) of 1.1 V, a J_{sc} of 17.14 mA cm^{-2}, and a fill factor (FF) of 60% gives a value of $\eta = 11\%$, this value matches the experimental results.[42,43] The current density characteristics of the $FAPbX_3$, and the $FAPb_{0.5}Sn_{0.25}Ge_{0.25}X_3$ compounds under AM1.5G solar irradiation are displayed in Fig. 5. $FAPb_{0.5}Sn_{0.25}Ge_{0.25}I_3$ has the highest current density with a value of 31.5 mA cm^{-2}. The short-circuit current density shows a monotonical decrease from $FAPb_{0.5}Sn_{0.25}Ge_{0.25}I_3$ to $FAPbCl_3$ that represents the lowest J_{sc}. In particular, the calculated short-circuit current density for the $FAPbX_3$ shows lower values regarding those of $FAPb_{0.5}Sn_{0.25}Ge_{0.25}X_3$ compounds, revealing that the doping of lead has largely improved the J_{sc}. On the other hand, the halogen (I, Br, Cl) variation increases the band gap enhancing the rise in open circuit voltage. The calculated open circuit voltage and the efficiency E_{loss} of 0.7 and 0.5 are listed in Table 3. Despite the high current density of $FAPb_{0.5}Sn_{0.25}Ge_{0.25}I_3$, this compound demonstrates the lowest efficiency among the three compounds due to its lower V_{oc} that can be improved by reducing the E_{loss}. Thus, as we can conclude from Fig. 5 and Table 3, a high short circuit current density is not the only parameter that determines the power of producing high efficiency. To summarize, Fig. 6 shows the variation of the efficiency as a function of the $FAPbX_3$, and $FAPb_{0.5}Sn_{0.25}Ge_{0.25}X_3$ bandgaps. $FAPb_{0.5}Sn_{0.25}Ge_{0.25}Cl_3$ reaches a high efficiency of 19.3% proving that this compound is a promising material for photovoltaic applications with low toxicity.

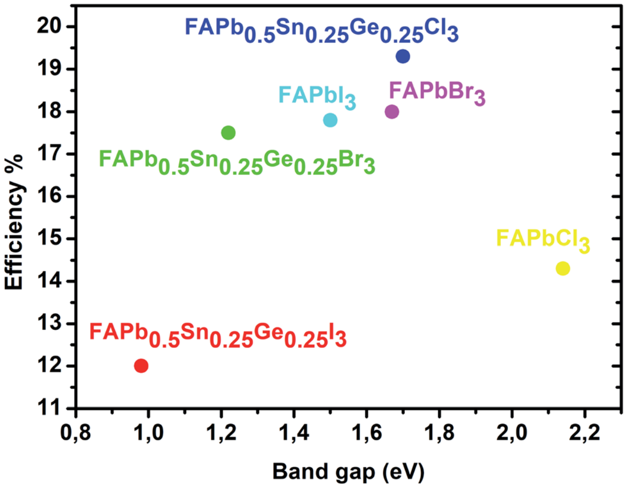

Fig. 6 Efficiency as a function of the $FAPbX_3$, and $FAPb_{0.5}Sn_{0.25}Ge_{0.25}X_3$ bandgaps.

4. Conclusion

In order to reduce the toxicity of the hybrid lead halide perovskite, the structural, electronic and optical properties of hybrids with less lead, perovskite $FAPb_{0.5}Sn_{0.25}Ge_{0.25}X_3$ (X = I, Br, Cl), are investigated using density functional theory and compared with those of $FAPbX_3$ (X = I, Br, Cl) compounds. The results show that the compounds have a suitable bandgap for photovoltaic cells. The evaluation of the photovoltaic parameters (J_{sc}, V_{oc}, FF, P_{in}) was carried out for the power conversion efficiency calculation. Results show that half doping of lead by both Ge and Sn, improves the stability of the system and enhances its performance for photovoltaic application. The adsorption coefficient and short-circuit current density have also been improved significantly with the doping effect, where the J_{sc} shows a monotonical increase from the $FAPbCl_3$ to $FAPb_{0.5}Sn_{0.25}Ge_{0.25}I_3$. We notice that, although the $FAPb_{0.5}Sn_{0.25}Ge_{0.25}I_3$ represents a high absorption coefficient in the visible range and the highest short-circuit current density, it represents the lowest power conversion efficiency due to its low open circuit voltage. $FAPb_{0.5}Sn_{0.25}Ge_{0.25}Cl_3$ has the highest power conversion efficiency demonstrating that this compound is promising for photovoltaic applications with low toxicity. This study can be a good reference for the development of new absorber materials in photovoltaic cells with lower toxicity and more efficiency.

Conflicts of interest

There are no conflicts to declare.

References

1 R. Ayres and V. Voudouris, The Economic Growth Enigma: Capital, Labour and Useful Energy?, *Energy Policy*, 2014, **64**(C), 16–28.

2 J. Eggoh, C. Bangaké and C. Rault, Energy Consumption and Economic Growth Revisited in African Countries, *Energy Policy*, 2011, **39**(11), 7408–7421.

3 J. Asafu-Adjaye, The Relationship between Energy Consumption, Energy Prices and Economic Growth: Time Series Evidence from Asian Developing Countries, *Energy Econ.*, 2000, **22**(6), 615–625.

4 R. York, Do Alternative Energy Sources Displace Fossil Fuels?, *Nat. Clim. Change*, 2012, **2**(6), 441–443, DOI: 10.1038/nclimate1451.

5 N. Kannan and D. Vakeesan, Solar Energy for Future World: – A Review, *Renewable Sustainable Energy Rev.*, 2016, **62**, 1092–1105, DOI: 10.1016/j.rser.2016.05.022.

6 K. Frohna and S. D. Stranks, 7 – Hybrid Perovskites for Device Applications, in *Handbook of Organic Materials for Electronic and Photonic Devices*, ed. Ostroverkhova, O., Woodhead Publishing Series in Electronic and Optical Materials, Woodhead Publishing, 2nd edn, 2019, pp. 211–256, DOI: 10.1016/B978-0-08-102284-9.00007-3.

7 A. K. Jena, A. Kulkarni and T. Miyasaka, Halide Perovskite Photovoltaics: Background, Status, and Future Prospects, *Chem. Rev.*, 2019, **119**(5), 3036–3103, DOI: 10.1021/acs.chemrev.8b00539.

8 H. B. Lee, N. Kumar, B. Tyagi, S. He, R. Sahani and J.-W. Kang, Bulky Organic Cations Engineered Lead-Halide Perovskites: A Review on Dimensionality and Optoelectronic Applications, *Mater. Today Energy*, 2021, **21**, 100759, DOI: 10.1016/j.mtener.2021.100759.

9 A. Boubekraoui, H. Moatassim, A. Al-Shami and H. Ez-Zahraouy, DFT Study of Structural, Electronic, and Thermoelectric Properties of $Cs_2PdX(X{=}Br_2Be_2Te_2)$ Compound, *Comput. Condens. Matter*, 2021, **29**, e00600, DOI: 10.1016/j.cocom.2021.e00600.

10 J. Jeong, M. Kim, J. Seo, H. Lu, P. Ahlawat, A. Mishra, Y. Yang, M. A. Hope, F. T. Eickemeyer, M. Kim, Y. J. Yoon, I. W. Choi, B. P. Darwich, S. J. Choi, Y. Jo, J. H. Lee, B. Walker, S. M. Zakeeruddin, L. Emsley, U. Rothlisberger, A. Hagfeldt, D. S. Kim, M. Grätzel and J. Y. Kim, Pseudo-Halide Anion Engineering for α-FAPbI 3 Perovskite Solar Cells, *Nature*, 2021, **592**(7854), 381–385, DOI: 10.1038/s41586-021-03406-5.

11 S. D. Stranks, G. E. Eperon, G. Grancini, C. Menelaou, M. J. P. Alcocer, T. Leijtens, L. M. Herz, A. Petrozza and H. J. Snaith, Electron-Hole Diffusion Lengths Exceeding 1 Micrometer in an Organometal Trihalide Perovskite Absorber, *Science*, 2013, **342**(6156), 341–344, DOI: 10.1126/science.1243982.

12 S. De Wolf, J. Holovsky, S.-J. Moon, P. Löper, B. Niesen, M. Ledinsky, F.-J. Haug, J.-H. Yum and C. Ballif, Organometallic Halide Perovskites: Sharp Optical Absorption Edge and Its Relation to Photovoltaic Performance, *J. Phys. Chem. Lett.*, 2014, **5**(6), 1035–1039, DOI: 10.1021/jz500279b.

13 G. E. Eperon, S. D. Stranks, C. Menelaou, M. B. Johnston, L. M. Herz and H. J. Snaith, Formamidinium Lead Trihalide: A Broadly Tunable Perovskite for Efficient Planar Heterojunction Solar Cells, *Energy Environ. Sci.*, 2014, **7**(3), 982–988, DOI: 10.1039/C3EE43822H.

14 S. R. Kumavat, Y. Sonvane, D. Singh and S. K. Gupta, Two-Dimensional $CH_3NH_3PbI_3$ with High Efficiency and Superior Carrier Mobility: A Theoretical Study, *J. Phys. Chem. C*, 2019, **123**(9), 5231–5239, DOI: 10.1021/acs.jpcc.8b11427.

15 T.-Y. Zhu and D.-J. Shu, Polarization-Controlled Surface Defect Formation in a Hybrid Perovskite, *J. Phys. Chem. Lett.*, 2021, **12**(16), 3898–3906, DOI: 10.1021/acs.jpclett.1c00702.

16 A. Babayigit, A. Ethirajan, M. Muller and B. Conings, Toxicity of Organometal Halide Perovskite Solar Cells, *Nat. Mater.*, 2016, **15**(3), 247–251, DOI: 10.1038/nmat4572.

17 J. Huang, S. Tan, P. D. Lund and H. Zhou, Impact of H_2O on Organic–Inorganic Hybrid Perovskite Solar Cells, *Energy Environ. Sci.*, 2017, **10**(11), 2284–2311, DOI: 10.1039/C7EE01674C.

18 A. Fakharuddin, F. De Rossi, T. M. Watson, L. Schmidt-Mende and R. Jose, Research Update: Behind the High Efficiency of Hybrid Perovskite Solar Cells, *APL Mater.*, 2016, **4**(9), 091505, DOI: 10.1063/1.4962143.

19 C. Li, S. Tscheuschner, F. Paulus, P. E. Hopkinson, J. Kießling, A. Köhler, Y. Vaynzof and S. Huettner, Iodine Migration and Its Effect on Hysteresis in Perovskite Solar Cells, *Adv. Mater.*, 2016, **28**(12), 2446–2454, DOI: 10.1002/adma.201503832.

20 M. Ouafi, B. Jaber, L. Atourki, R. Bekkari and L. Laânab, Improving UV Stability of $MAPbI_3$ Perovskite Thin Films by Bromide Incorporation, *J. Alloys Compd.*, 2018, **746**, 391–398, DOI: 10.1016/j.jallcom.2018.02.240.

21 H. Moatassim, A. El Kenz, A. Benyoussef, M. Loulidi and O. Mounkachi, Degradation Mechanism of $CH_3NH_3PbI_3$ and Enhancing Its Optical Absorption through Variety of Doping Sites, *Comput. Condens. Matter*, 2021, **29**, e00611, DOI: 10.1016/j.cocom.2021.e00611.

22 C. Wu, D. Guo, P. Li, S. Wang, A. Liu and F. Wu, A Study on the Effects of Mixed Organic Cations on the Structure and Properties in Lead Halide Perovskites, *Phys. Chem. Chem. Phys.*, 2020, **22**(5), 3105–3111, DOI: 10.1039/C9CP06182G.

23 A. Oranskaia, J. Yin, O. M. Bakr, J.-L. Brédas and O. F. Mohammed, Halogen Migration in Hybrid Perovskites: The Organic Cation Matters, *J. Phys. Chem. Lett.*, 2018, **9**(18), 5474–5480, DOI: 10.1021/acs.jpclett.8b02522.

24 X. Zhang, J.-X. Shen, M. E. Turiansky and C. G. Van de Walle, Minimizing Hydrogen Vacancies to Enable Highly Efficient Hybrid Perovskites, *Nat. Mater.*, 2021, **20**(7), 971–976, DOI: 10.1038/s41563-021-00986-5.

25 M. Lyu, J.-H. Yun, P. Chen, M. Hao and L. Wang, Addressing Toxicity of Lead: Progress and Applications of Low-Toxic Metal Halide Perovskites and Their Derivatives, *Adv. Energy Mater.*, 2017, **7**(15), 1602512, DOI: 10.1002/aenm.201602512.

26 J. Prakash, A. Singh, G. Sathiyan, R. Ranjan, A. Singh, A. Garg and R. K. Gupta, Progress in Tailoring Perovskite Based Solar Cells through Compositional Engineering: Materials Properties, Photovoltaic Performance and Critical Issues, *Mater. Today Energy*, 2018, **9**, 440–486, DOI: 10.1016/j.mtener.2018.07.003.

27 L. Peng and W. Xie, Theoretical and Experimental Investigations on the Bulk Photovoltaic Effect in Lead-Free Perovskites $MASnI_3$ and $FASnI_3$, *RSC Adv.*, 2020, **10**(25), 14679–14688, DOI: 10.1039/D0RA02584D.

28 T. Krishnamoorthy, H. Ding, C. Yan, W. L. Leong, T. Baikie, Z. Zhang, M. Sherburne, S. Li, M. Asta, N. Mathews and S. G. Mhaisalkar, Lead-Free Germanium Iodide Perovskite Materials for Photovoltaic Applications, *J. Mater. Chem. A*, 2015, **3**(47), 23829–23832, DOI: 10.1039/C5TA05741H.

29 D. Liu, Q. Li, J. Hu, R. Sa and K. Wu, Photovoltaic Performance of Lead-Less Hybrid Perovskites from Theoretical Study, *J. Phys. Chem. C*, 2019, **123**(20), 12638–12646, DOI: 10.1021/acs.jpcc.9b02705.

30 P. Giannozzi, S. Baroni, N. Bonini, M. Calandra, R. Car, C. Cavazzoni, D. Ceresoli, G. L. Chiarotti, M. Cococcioni, I. Dabo, A. Dal Corso, S. de Gironcoli, S. Fabris, G. Fratesi, R. Gebauer, U. Gerstmann, C. Gougoussis, A. Kokalj, M. Lazzeri, L. Martin-Samos, N. Marzari, F. Mauri, R. Mazzarello, S. Paolini, A. Pasquarello, L. Paulatto, C. Sbraccia, S. Scandolo, G. Sclauzero, A. P. Seitsonen, A. Smogunov, P. Umari and R. M. Wentzcovitch, QUANTUM ESPRESSO: A Modular and Open-Source Software Project for Quantum Simulations of Materials, *J. Phys.: Condens. Matter*, 2009, **21**(39), 395502, DOI: 10.1088/0953-8984/21/39/395502.

31 J. Klimeš, D. R. Bowler and A. Michaelides, Van Der Waals Density Functionals Applied to Solids, *Phys. Rev. B: Condens. Matter Mater. Phys.*, 2011, **83**(19), 195131, DOI: 10.1103/PhysRevB.83.195131.

32 Y. Wang, T. Gould, J. F. Dobson, H. Zhang, H. Yang, X. Yao and H. Zhao, Density Functional Theory Analysis of Structural and Electronic Properties of Orthorhombic Perovskite $CH_3NH_3PbI_3$, *Phys. Chem. Chem. Phys.*, 2013, **16**(4), 1424–1429, DOI: 10.1039/C3CP54479F.

33 D. Sangalli, A. Ferretti, H. Miranda, C. Attaccalite, I. Marri, E. Cannuccia, P. Melo, M. Marsili, F. Paleari, A. Marrazzo, G. Prandini, P. Bonfà, M. O. Atambo, F. Affinito, M. Palummo, A. Molina-Sánchez, C. Hogan, M. Grüning, D. Varsano and A. Marini, Many-Body Perturbation Theory Calculations Using the Yambo Code, *J. Phys.: Condens. Matter*, 2019, **31**(32), 325902, DOI: 10.1088/1361-648X/ab15d0.

34 J. Wu, G. Yue, Y. Xiao, J. Lin, M. Huang, Z. Lan, Q. Tang, Y. Huang, L. Fan, S. Yin and T. Sato, An Ultraviolet Responsive Hybrid Solar Cell Based on Titania/Poly(3-Hexylthiophene), *Sci. Rep.*, 2013, **3**(1), 1283, DOI: 10.1038/srep01283.

35 M. A. Green, Solar Cell Fill Factors: General Graph and Empirical Expressions, *Solid-State Electron.*, 1981, **24**(8), 788–789, DOI: 10.1016/0038-1101(81)90062-9.

36 M. R. Filip, C. Verdi and F. Giustino, GW Band Structures and Carrier Effective Masses of $CH_3NH_3PbI_3$ and Hypothetical Perovskites of the Type $APbI_3$: $A = NH_4$, PH_4, AsH_4, and SbH_4, *J. Phys. Chem. C*, 2015, **119**(45), 25209–25219, DOI: 10.1021/acs.jpcc.5b07891.

37 N. Baaalla, Y. Ammari, E. K. Hlil, R. Masrour, A. E. Kenz and A. Benyoussef, Study of Optical, Electrical and Photovoltaic Properties of $CH_3NH_3PbI_3$ Perovskite: *Ab Initio* Calculations, *Phys. Scr.*, 2020, **95**(9), 095104, DOI: 10.1088/1402-4896/abae1e.

38 X.-F. Diao, Y. Tang, T. Tang, Q. Xie, K. Xiang and G. Liu, Study on the Stability of Organic–Inorganic Perovskite Solar Cell Materials Based on First Principle, *Mol. Phys.*, 2020, **118**(8), e1665200, DOI: 10.1080/00268976.2019.1665200.

39 C. C. Stoumpos, C. D. Malliakas and M. G. Kanatzidis, Semiconducting Tin and Lead Iodide Perovskites with Organic Cations: Phase Transitions, High Mobilities, and Near-Infrared Photoluminescent Properties, *Inorg. Chem.*, 2013, **52**(15), 9019–9038, DOI: 10.1021/ic401215x.

40 X. Qian, X. Gu and R. Yang, Lattice Thermal Conductivity of Organic–Inorganic Hybrid Perovskite $CH_3NH_3PbI_3$, *Appl. Phys. Lett.*, 2016, **108**(6), 063902, DOI: 10.1063/1.4941921.

41 L. Leppert, S. E. Reyes-Lillo and J. B. Neaton, Electric Field- and Strain-Induced Rashba Effect in Hybrid Halide Perovskites, *J. Phys. Chem. Lett.*, 2016, **7**(18), 3683–3689, DOI: 10.1021/acs.jpclett.6b01794.

42 P. Fan, D. Gu, G.-X. Liang, J.-T. Luo, J.-L. Chen, Z.-H. Zheng and D.-P. Zhang, High-Performance Perovskite $CH_3NH_3PbI_3$ Thin Films for Solar Cells Prepared by Single-Source Physical Vapour Deposition, *Sci. Rep.*, 2016, **6**(1), 29910, DOI: 10.1038/srep29910.

43 D. Liu, M. K. Gangishetty and T. L. Kelly, Effect of $CH_3NH_3PbI_3$ Thickness on Device Efficiency in Planar Heterojunction Perovskite Solar Cells, *J. Mater. Chem. A*, 2014, **2**(46), 19873–19881, DOI: 10.1039/C4TA02637C.